POAC '99
Espoo, Finland

Proceedings of the 15th
International Conference on
Port and Ocean Engineering
under Arctic Conditions

A CALCULATION OF ICE LOADS ON THE DWL OF THE SWEDISH COAST GUARD SHIP KBV-181 AND CORRESPONDING MEASUREMENTS WITH THE MS UISKO

P. Valanto
Hamburg Ship Model Basin HSVA, Germany

ABSTRACT

A 3-D numerical model of the icebreaking process on the load waterline of a ship advancing in level ice was used to investigate the magnitude of the ice loads on the DWL of the Swedish Coast Guard Ship KBV-181. The ice loads computed for level ice were compared with measurements on a sister ship MS Uisko having a somewhat shorter parallel midship, but an identical forebody and bow. These high-quality measurements were used to investigate the accuracy and reliability of the computed results. The correlation between the computed deterministic results and the measured short term ice loads is very satisfactory. The dependency of the computed ice loads on ship speed and ice thickness is shown to be very similar to those of the measurements. This gives the possibility numerically to investigate ice loads on the DWL as a function of ship speed and ice thickness with a good reliability. This information can be used to give guidelines for vessels occasionally traveling in ice covered waters on how to proceed safely. Examples of such vessels are many naval and governmental vessels traveling in relatively light or moderate ice conditions under limited duration of time.

1. INTRODUCTION

Ice loads on the design waterline of the Swedish Coast Guard Ship KBV-181 advancing in level ice were computed. For this purpose the icebreaking process at the side of the ship was numerically simulated. The time history of the contact forces, the duration of the contact and the minimum required ship-ice contact area were determined. The ice loads on 5 segments on the DWL were computed for some values of ice thickness and ship speed. The computed ice loads for level ice were compared with measurements on a sister ship MS Uisko having a somewhat shorter parallel midship, but an identical forebody and bow. These high-quality measurements (Kivimaa, 1993) were used to investigate the accuracy and reliability of the computed results.

Figure 1 shows a sketch of the MS Uisko and the location of the ice load panel (900 mm x 1350 mm) in the bow just at the waterline. The DWL-length of the MS Uisko is 45.4 m, draught 4.1 m at midships and breadth 10.2 m. The total displacement is 850 tons. The ship is powered by two Wärtsilä diesel engines with the total nominal power of 2360 kW (Kivimaa, 1993). The KBV-181 has a longer midship section and thus a somewhat higher DWL-length of 51.4 m, draught 4.3 m at midships and breadth 10.2 m. The ship is powered by two main engines with the total nominal power of 2840 kW (Dagnevik, 1998).

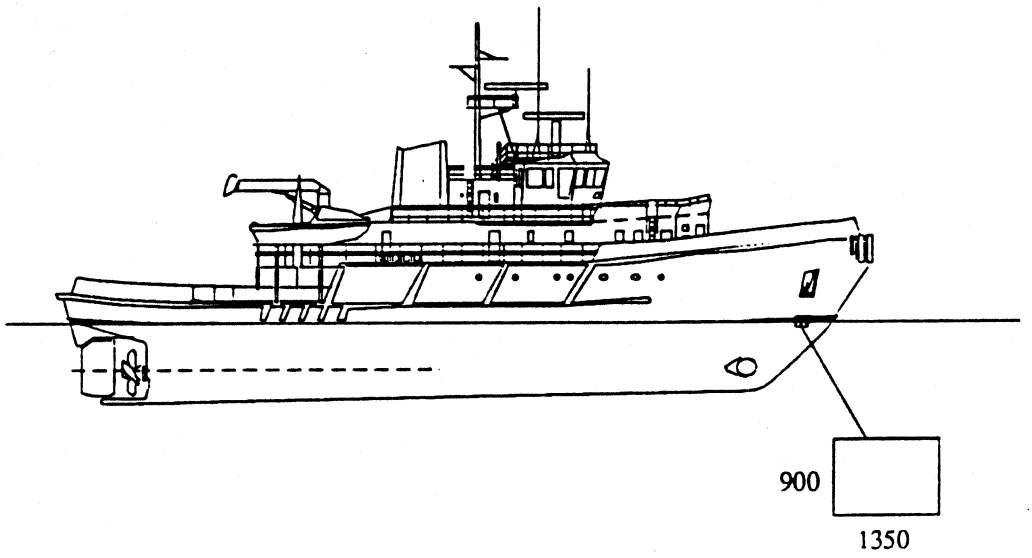

Fig. 1 MS Uisko and the location of the ice load panel (Kivimaa, 1993).

2. A NUMERICAL MODEL OF THE ICEBREAKING PROCESS AT THE DWL

A numerical model for simulating the response of a floating ice cover and the surrounding fluid to an advancing ship hull is briefly described. The theory behind the numerical model is based on the assumption of unsteady potential flow together with a relatively complicated dynamic boundary condition on the ice cover – fluid surface. Contrary to many workers in the field we do not solve a plate equation describing the behavior of the ice cover, but the equation of the fluid motion and use the plate equation only as a boundary condition. This allows a very complete modeling of the icebreaking process at the bow of the ship advancing in level ice. A non-linear load function is used to describe the contact force due to the advance of the vessel and the response of the ice cover. The behavior of the floating ice cover and that of the broken floe is modeled up to the moment the vessel has advanced the length of the broken floe. At this moment the broken ice floe has rotated parallel to the bow of the advancing vessel. After this a new icebreaking cycle starts.

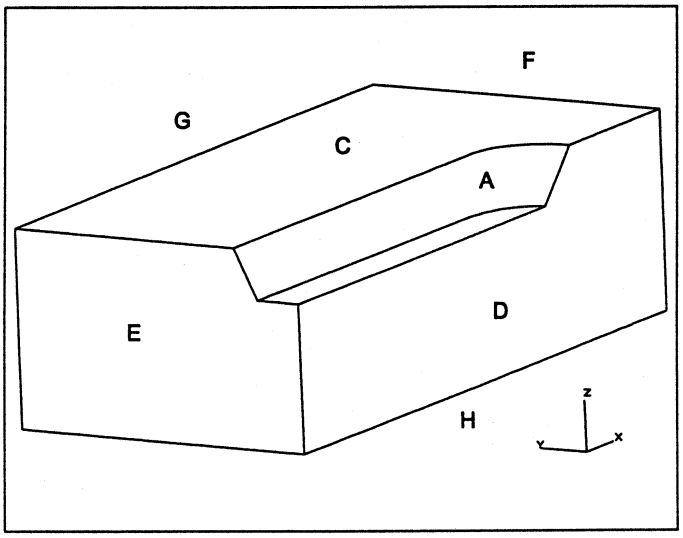

Fig. 2 Geometry of the physical fluid domain.

The domain to be modeled consists of the floating ice cover, the water beneath, and the advancing ship hull. Due to reasons of symmetry only the left side of the vessel is modeled. Figure 2 illustrates the geometry of the fluid domain. The fluid is assumed incompressible and inviscid, and the flow irrotational. The fluid disturbance at time t is described by a velocity potential $\phi(x, y, z, t)$, with the fluid velocity given by $\nabla\phi$. It is well known that ϕ is a

solution of Laplace´s equation and that the momentum equations yield Euler´s integral. Hence,

$$\nabla^2\phi(x,y,z,t)=0 \quad , \tag{1}$$

$$\frac{p(x,y,z,t)}{\rho}+\frac{\partial\phi}{\partial t}+\frac{1}{2}\nabla\phi\cdot\nabla\phi+gz=0 \quad , \tag{2}$$

where p is the fluid pressure, ρ the density of the fluid, and g the acceleration due to gravity.

It is generally known that sea ice as a material behaves in two different ways. Depending on strain rate and temperature, the behavior of the ice is either elastic with brittle failure or viscoelastic with ductile failure. In the case of interaction between ship and ice in the forward region of a ship hull, the strain rate is high enough for the behavior to be considered linearly elastic and brittle. This allows us to use a linear constitutive equation in the numerical model. In addition, the material of the floating ice cover is assumed homogeneous and isotropic.

The kinematic boundary conditions on the ice cover – fluid surface (C) can be obtained by noting that this surface, described by $z=\zeta(x,y,t)$, is a material surface. As the sea ice as a material is very rigid in comparison with its flexural strength, the deflections ζ will be very small. Because of this, the boundary conditions on (C) can be satisfied on the surface $z=0$, that is, on the reference position of the ice cover. Hence, the kinematic boundary condition on the ice cover–fluid surface (C) becomes

$$\zeta_{,t}-\phi_{,z}=0 \qquad \text{on C.} \tag{3}$$

The dynamic ice cover-fluid condition results from the equations of equilibrium in translation normal to the ice cover and in rotation: The equations of equilibrium for an infinitesimal piece of the floating ice plate give, in the transversal direction,

$$Q^{\alpha}|_{\alpha}-h_i\rho_i\zeta_{,tt}+p+q=0 \quad , \tag{4}$$

where Q^{α} is the shear force component acting in section x^{α} is constant, h_i the thickness and ρ_i the density of the ice cover. The vertical line in the equation designates covariant differentiation and the repeated index implies summatum, getting values 1, 2. The second term describes the inertia of the ice plate, p is the fluid pressure, and q the external load on the plate. The equations of equilibrium give for rotation

$$M^{\alpha\beta}|_{\beta}-Q^{\alpha}=0 \quad , \tag{5}$$

where $M^{\alpha\beta}$ is the bending moment. Differentiating (5) with respect to x^{α} and using (4) we get

$$M^{\alpha\beta}|_{\alpha\beta}-h_i\rho_i\zeta_{,tt}+p+q=0 \quad , \tag{6}$$

The moment $M^{\alpha\beta}$ is related to the second derivative of the deflection

$$M^{\alpha\beta}=-D[(1-\nu)\zeta|^{\alpha\beta}+\nu\zeta|^{\gamma}_{\gamma}\,g^{\alpha\beta}] \quad , \tag{7}$$

in which the $g^{\alpha\beta}$ is the contravariant component of metric tensor and the quantity D is the flexural rigidity of the ice plate $D = Eh_i^3 / 12(1-\upsilon^2)$, where ν is Poisson´s ratio. This yields

$$-D\zeta\,|^{\alpha\beta}_{\alpha\beta} - h_i\rho_i\zeta_{,tt} + p + q = 0 \quad , \tag{8}$$

which is identical to

$$-D\nabla^4\zeta - h_i\rho_i\zeta_{,tt} + p + q = 0 \quad . \tag{9}$$

Substituting Euler´s integral to (9) we get

$$\frac{D\phi}{Dt} = -\frac{D}{\rho}\nabla^4\zeta - \frac{h_i\rho_i}{\rho}\zeta_{,tt} + \vec{v}\cdot\nabla\phi - \frac{1}{2}\nabla\phi\cdot\nabla\phi - g\zeta + \frac{q}{\rho} \quad , \tag{10}$$

where ρ is the fluid density, and q the external surface load on the ice cover. Before flexural failure the vector $\vec{v}$ has the form $(0,0,\zeta_{,t})$, and the equation (10) yields (11). In this case the dynamic boundary condition (11) is applied on the whole length of the floating cover. Hence,

$$\frac{D\phi}{Dt} = -\frac{D}{\rho}\nabla^4\zeta - \frac{h_i\rho_i}{\rho}\zeta_{,tt} + \frac{1}{2}(-\phi_{,x}^2 - \phi_{,y}^2 + \phi_{,z}^2) - g\zeta + \frac{q}{\rho} \quad , \quad \text{on C.} \tag{11}$$

After flexural failure the equation (11) is applied on the unbroken part of the floating cover (C). On the rotating floe (B) the displacements are large, and the boundary points are updated at each time step. The dynamic boundary condition on the rotating floe becomes

$$\frac{D\phi}{Dt} = -\frac{D}{\rho}\nabla^4\zeta - \frac{h_i\rho_i}{\rho}\frac{D^2\zeta}{Dt^2} + \vec{v}\cdot\nabla\phi - \frac{1}{2}\nabla\phi\cdot\nabla\phi - g(\zeta + t_f)\cos(\theta) + \frac{q}{\rho} \quad , \text{ on B,} \tag{12}$$

where the vector $\vec{v} = (x_{,t}, y_{,t}, z_{,t})$, and θ is the angle of rotation. The quantity t_f is the depth of fluid on top of the rotating floe. This fluid is related to partial ventilation taking place during the rotation phase. The surface load q in (11) and (12) is non-zero only in the first row of nodes on the floating ice cover or on the broken floe at the waterline of the ship bow and describes the transversal component F_ζ of the contact force resulting from the advance of the vessel. The forces in the contact surface develop a non-zero moment with respect to the neutral axis of the ice plate. This bending moment M_{nn} shows in the numerical expression of the bi-Laplacian ($\nabla^4\zeta$) in equations (11) and (12) at the end of the floating ice cover or the broken floe. Equation (1) with boundary conditions typical to pure fluid flow problems (Dirichlet, Neumann, Sommerfeld) and with (11)-(12) define the nonlinear initial/boundary-value problem of the motion of the fluid and the deflection of the floating ice cover.

The boundary of the floating ice cover is at contact points on the ship waterline loaded by the advancing ship hull. As the vessel advances, the edge of the ice cover is partially crushed.

The resulting contact force causes the edge of the ice cover to deflect downwards, and in principle to compress in horizontal direction. The resulting in-plane displacements appear to be relatively small and can be omitted from the contact model. The resulting in-plane stresses are compressive, they reduce the tensile stresses in the top layer of the ice cover due to bending and thus postpone the flexural failure in the ice cover. Due to typical hull angles on the ship shoulders the compressive in-plane stresses can become higher than the flexural stress. This can lead to a situation, where the failure mode shifts from cusp breaking to crushing and shearing on the ship shoulders. In the numerical model the in-plane stresses are computed separately based on a numerical solution of Airy´s stress function and combined with the flexural stresses to give the stress state in the ice cover accurately, as shown in Fig. 3.

The contact area between the ship hull and the ice cover is calculated based on the geometric difference between the steady advance of the ship hull (rigid indentor) and the response of the ice cover. The contact force is then defined as

$$F_n = f_{ic} A_c \sigma_c \qquad (13)$$

where F_n is the normal force, f_{ic} the contact coefficient, A_c the contact area, and σ_c the uniaxial unconfined compressive strength of ice. Mechanical friction forces will be present on the contact surface during the crushing process, Coulomb type (dry) friction is assumed to be present. The only (one) empirical coefficient in the numerical model is the contact coefficient f_{ic}, which has the value of 0.5 for the ship hull - full scale level ice contact in the numerical model. This simple model has its limitations: It is too coarse for computing the local contact pressure variations inside the contact area on the shell plate itself, but it can be successfully used as a model in computing the maximum contact loads, which are dominated by the hydrodynamic effects.

3. SOLUTION METHOD

It is evident that the treatment of the field equation in a potential formulation (1) is relatively straightforward. As in free-surface problems, the difficulties arise in determining the ice cover – fluid surface location simultaneously with the satisfaction of the boundary conditions and the field equation. In comparison with the free-surface boundary conditions, the dynamic boundary conditions (11) and (12) have two important additional terms: the fourth spatial derivative $(\nabla^4 \zeta)$ and the second derivative $(\zeta_{,tt})$ of ζ in time. These terms require a considerably smaller time step than otherwise would be needed for convergence.

Like the coordinate transformation equations needed for the boundary-fitted coordinate system used, also the transformed field equation is solved iteratively with the SOR-method speeded up by a multi-grid algorithm. A second-order accurate finite difference scheme with a time-dependent boundary-fitted coordinate system is used to solve the field equation in the changing physical fluid domain. The initial value approach has the advantage that the conditions on the moving ice cover – fluid boundary can be used to advance the solution in time. During each time step, new values of ζ and ϕ on the ice cover – fluid boundary are advanced with the 4´th order Adams-Moulton Predictor-Corrector Method.

Regardless of the mentioned problem with the term with the second time derivative describing the ice cover inertia, the method used produces remarkably good results. Further, at the early stages of the indentation the inertia of the ice cover itself is practically negligible in comparison to the fluid inertia. For a rapid indentation, the ice cover may be treated as a

massless elastic plate on a fluid foundation. The term related to ice cover inertia disappears and the dynamic boundary condition (11) becomes

$$\frac{D\phi}{Dt} = -\frac{D}{\rho}\nabla^4\zeta + \frac{1}{2}(-\phi_{,x}^2 - \phi_{,y}^2 - \phi_{,z}^2) - g\zeta + \frac{q}{\rho} \quad , \quad on\ C. \tag{14}$$

The dynamic boundary condition (12) on the broken floe becomes

$$\frac{D\phi}{Dt} = -\frac{D}{\rho}\nabla^4\zeta + \vec{v}\cdot\nabla\phi - \frac{1}{2}\nabla\phi\cdot\nabla\phi - g(\zeta + t_f)\cos(\theta) + \frac{q}{\rho} \quad , \quad on\ B. \tag{15}$$

Results from 2-D calculations indicate that the simplified boundary conditions can be used with a good accuracy until the flexural failure takes place in the sheet, and after that as a good approximation, when a faster numerical solution for the whole icebreaking cycle is required (Valanto, 1992). The cpu-time used for the numerical solution with the simplified boundary conditions was only 33 percent of that used with the original computation with full boundary conditions. In the present study the simplified boundary conditions are used.

The numerical solution of the whole icebreaking cycle consists of two parts: (1) the time integration of the solution before the (global) flexural failure occurs in the cover; (2) The time integration of the solution after flexural failure has taken place, during the rotation of the broken floe. The main differences between the two parts are the load formulations and the updating of the geometry of the fluid domain. Part (1) continues until flexural failure in the ice cover is reached, that is, until the principal stress σ_1 in the ice cover exceeds the flexural strength σ_f of the ice cover. The principal stress σ_1 is a combination of stress due to bending of the cover and (compressive) in-plane stress $(\sigma_{cx}, \sigma_{cy}, \tau_{cxy})$ in the horizontal direction,

$$\sigma_x = -\frac{Eh_i}{2(1-\nu^2)}(\zeta_{,xx} + \nu\zeta_{,yy}) + \sigma_{cx} \quad , \tag{16}$$

$$\sigma_y = -\frac{Eh_i}{2(1-\nu^2)}(\zeta_{,yy} + \nu\zeta_{,xx}) + \sigma_{cy} \quad , \tag{17}$$

$$\tau_x = -\frac{Eh_i}{2(1+\nu)}\zeta_{,xy} + \tau_{cxy} \quad . \tag{18}$$

Expressions for $\zeta_{,xx}$, $\zeta_{,yy}$, and $\zeta_{,xy}$ in curvilinear coordinates can be found in the reference (Thompson, 1985). The principal stresses are given by

$$\sigma_{1,2} = \frac{(\sigma_x + \sigma_y)}{2} \pm \frac{1}{2}\sqrt{(\sigma_x - \sigma_y)^2 + 4\tau_{xy}^2} \quad . \tag{19}$$

The length of the broken floe is calculated from the location of maximum principal stress in the cover. When the principal stress exceeds the flexural strength, flexural failure is assumed to take place instantly and completely *in that grid point*. Thus at the side of the ship bow, when the stress level in the ice cover has become high, a local failure starts to propagate rapidly as the ship advances. The ice floe is broken off, when the principal stresses exceed the strength in the last grid points connecting the floe to the rest ice plate, which leads into a

global failure of the ice cover in front or at the side of the bow. At the next step, the routines of the program part (2) are used. The numerical time integration ends when the floe has reached the velocity required by the advance of the ship and the ship-ice contact breaks momentarily off.

Previous experiences with the numerical model in computing full scale breaking patterns (Valanto, 1993) show that *stresses in sea ice also under slow loading rate can be calculated with a linearly elastic material model together with a simple failure criterion, in order to predict the size and shape of the broken ice floes.* Accurate prediction of these two is a prerequisite for accurate computation of the maximum ice loads.

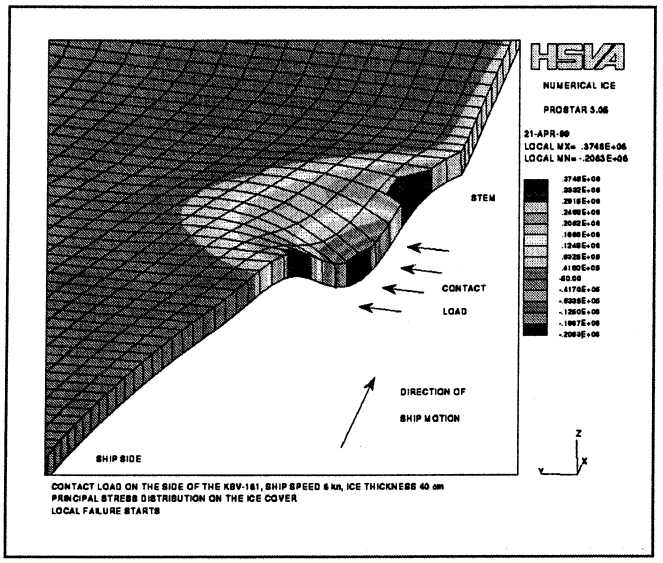

Fig. 3 Principal stress distribution on the ice cover beside the KBV-181. Max. ice load 160 kN/m, duration of the contact 0.049 s.

The numerical model shows that *already at relatively slow speeds the maximum (horizontal) force is not reached when the ice floe breaks completely free, but considerably later, when the broken ice floe and its hydrodynamic mass have reached the velocity required by the steady forward motion of the ship.* Thus the global ice failure only limits the horizontal extent of the ice cover to be accelerated, from the whole ice cover strictly to the ice floe only. The location where the global ice failure takes place and the ice cover breaks has a strong effect on the maximum horizontal force, through the determination of the horizontal extent of the ice cover and its hydrodynamic mass to be accelerated.

4. COMPUTATION OF THE ICE LOADS ON THE DWL OF THE SWEDISH COAST GUARD SHIP KBV-181

Ice loads on the design waterline of the Coast Guard Ship KBV-181 advancing in level ice were computed with the 3-D model originally developed for purposes of ice resistance prediction. The time history of the contact forces, the duration of the contact and the minimum contact area were determined. The ice loads on the segment corresponding MS Uisko´s panel on the DWL were computed for several values of ship speed and level ice thickness. Such computed results form a good data for structural analysis of the frames and larger structures of the ship in the mentioned ice conditions. The accurate distribution of the peak ice pressure on the shell plate between the frames is too small a detail for the numerical model

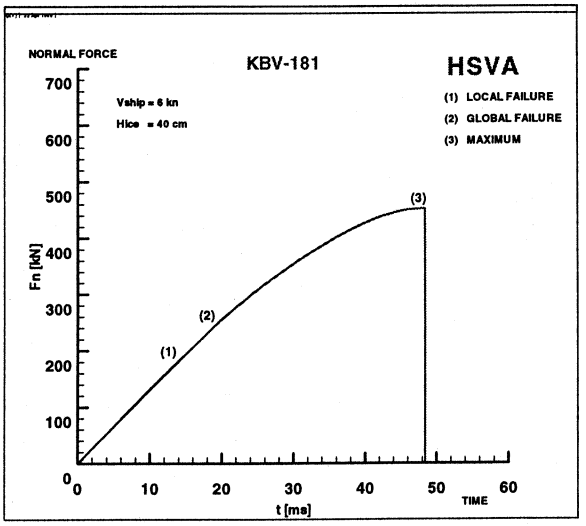

Fig. 4 Time-history of the normal component of the contact force.

used. The integral of this ice pressure distribution, that is, the ice load itself, is predicted well.

The computed contact force has a normal and a tangential component to the ship shell on the DWL. The tangential component is to great extent caused by friction and is important for ship resistance in level ice. The normal component is the most important one for ice loads on the hull. An example of the time-histories of the contact forces is given in Figure 4. The numbers in the figure indicate the moments on the time-history of the normal force, where (1) the local failure in the ice cover starts, (2) the floe is broken off (global failure), (3) the floe together with its hydrodynamic mass has reached the speed required by the steady forward motion of the ship. Notice the relatively large distance, and work done after floe breaking, between the points (1-2) and on the other hand point (3).

5. MEASUREMENTS OF ICE LOADS ON MS UISKO

The measurements were conducted over two winter seasons 1988-1989 in the Baltic Sea in various ice conditions (Kivimaa, 1993). A load panel of 0.9 m x 1.35 m was developed and installed to the bow structure of the cutter MS Uisko for this purpose. Both the normal and tangential components of the ice forces acting on the panel were measured. Dedicated trials were made in level ice in addition to the long-term measurements. In connection with the trials besides the ice thickness, also the flexural strength of the ice cover was measured with cantilever beam tests, and the uniaxial unconfined compressive strength with prismatic samples (9 cm x 9 cm x 20 cm) using a hydraulic testing machine resulting in strain rate of 10^{-3}. Altogether 12 ice beams and 22 prismatic samples were tested.

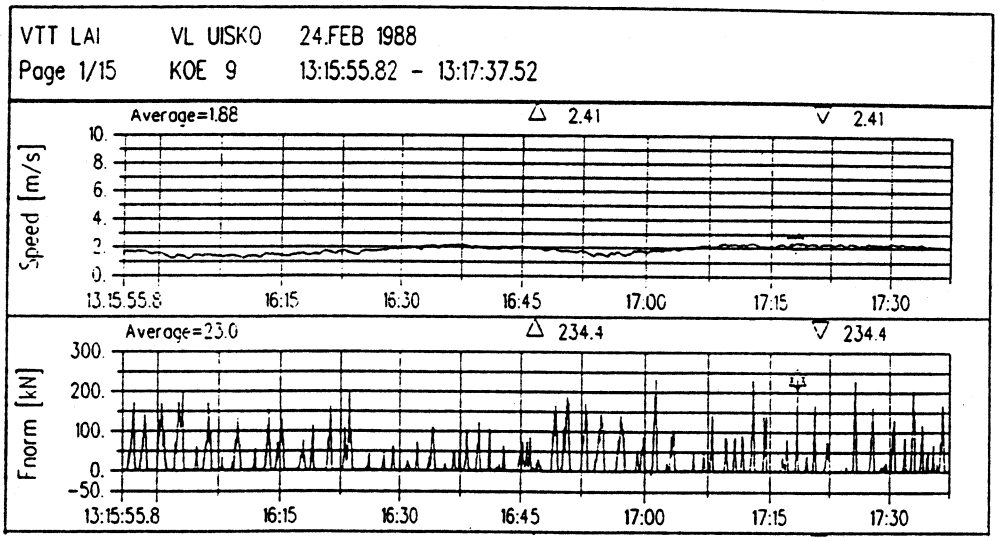

Fig. 5 A sample time history of the MS Uisko panel normal ice force in level ice (Kivimaa, 1993).

Figure 5 (Kivimaa, 1993) illustrates a typical normal force time signal of the ice load panel in level ice. According to Kivimaa the ice thickness in the illustrated test was 51 cm and the average ship speed 1.9 m/s. The panel encountered ice impacts with the frequency of 0.6 Hz. From this we can calculate that the ship advanced approximately 3.167 m in the 51 cm thick ice between the recorded impacts, which we assume to be related to the breaking of

ice floes. MS Uisko has a waterline angle of about 30° in the panel area, which gives for the normal distance between the load impacts, that is, for the normal length of the ice floe the value 1.6 m. This results in floe length to ice thickness ratio of 3.14. Other full scale measurements give the values of 2.2-4.4 to this ratio, depending on speed, so that lower values are obtained at higher speeds and vice versa (Valanto, 1993). The value 3.14 fits into this range very well, which supports the conclusion that the measured load peaks indeed are closely related to cyclic breaking of ice floes.

6. COMPARISON OF COMPUTED AND MEASURED ICE LOADS

In the computations we have used the values of ice thickness measured in the test ice fields (Kivimaa, 1993) and flexural and crushing strength values from the same reference, but increased the strength values with two standard deviations estimated according to Kujala (1994). With this an attempt is made better to catch the *peak loads* measured with the MS

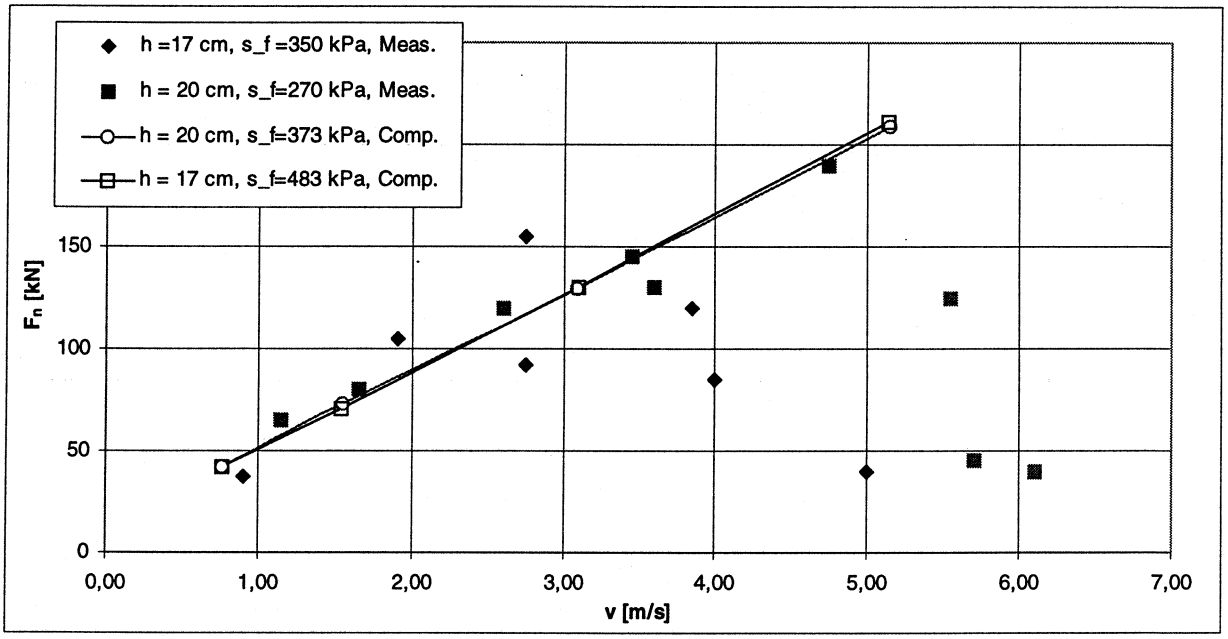

Fig. 6 Comparison of peak loads measured with MS Uisko and computed for KBV-181.

Uisko in the level ice fields. Figure 6 shows the computed and the measured peak forces as a function of ship speed. The effect of the higher strength values used in the computation is small (ca. 7 percent), but the coarse numerical grid may have a lowering effect on the computed results. Altogether the correlation between the computed deterministic results and the measured short term ice loads is very satisfactory. According to Kivimaa (1993) the clear decrease in the peak forces at high speeds over 5 m/s indicates that at higher speeds the panel did not crush and break undamaged ice, but the ice edge was broken prior to the contact with the panel by a rather significant bow wave of the vessel. At lower speeds the dependency of the computed ice loads on ship speed is very similar to that of the measurements.

The computations by Valanto (1995) show further that the natural variation of the compressive strength of the ice, used in modeling the contact between the ship side and the ice cover, appears to cause only relatively small changes in the peak loads in comparison with changes caused by the ice thickness or ship speed. This is due to the dominance of

hydrodynamic effects in the early parts of the icebreaking process, during which the peak loads are reached. All this gives the possibility to investigate ice loads on the DWL as a function of ship speed and ice thickness with a good reliability.

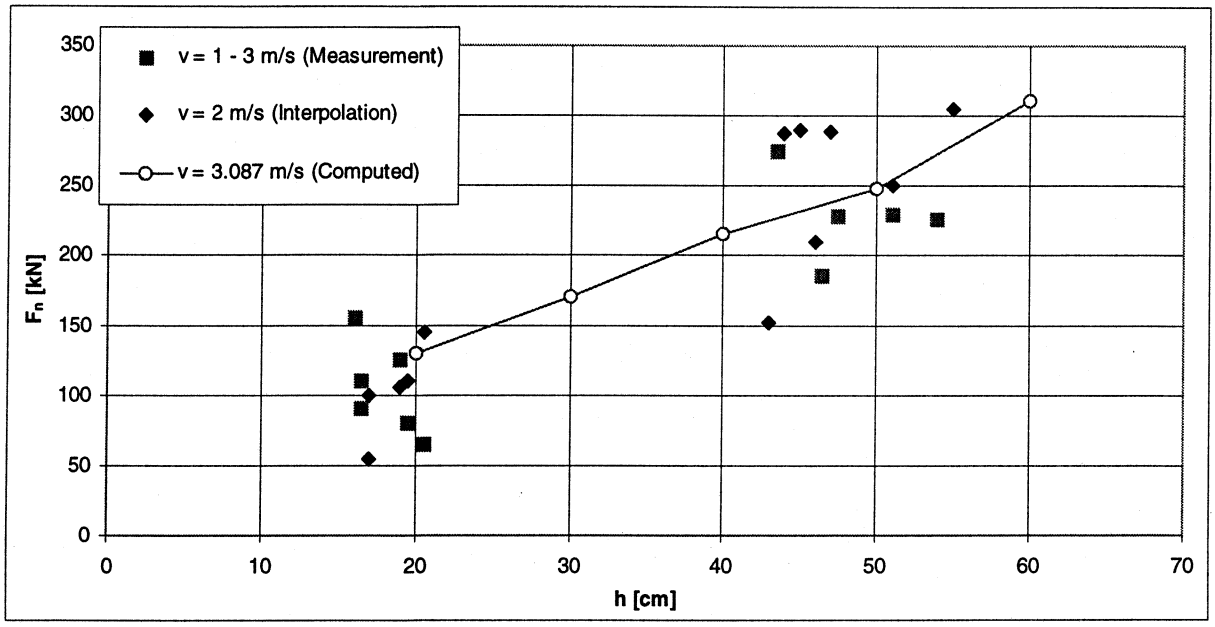

Fig. 7 Comparison of the peak loads measured with MS Uisko and computed for KBV-181 with different values of ice thickness.

Figure 7 shows the dependency of the normal component of the contact force measured by the panel as a function of ice thickness. Also in this case the correlation between the measured and computed load peaks is very satisfactory. Careful analysis of experiments with model ice and corresponding computations show that the influence of variations in the flexural and crushing strengths on the peak loads can be computed with a good reliability (Valanto, 1995). Thus the effects of the three most important factors influencing the peak load, namely, *ice thickness, ice strength,* and *ship speed*, can be well modeled.

The peak load *distribution* along the DWL depends on the hull angles on the waterline. These influence (1) the force geometry at the contact point and (2) the hull normal velocity against the edge of the ice cover. Modeling these purely geometrical factors correctly in the numerical model is of no great difficulty.

Figure 8 shows an example of such a peak load distribution on the DWL of the KBV-181 in 20 cm thick level ice with the speeds of 3, 6, and 10 kn. The

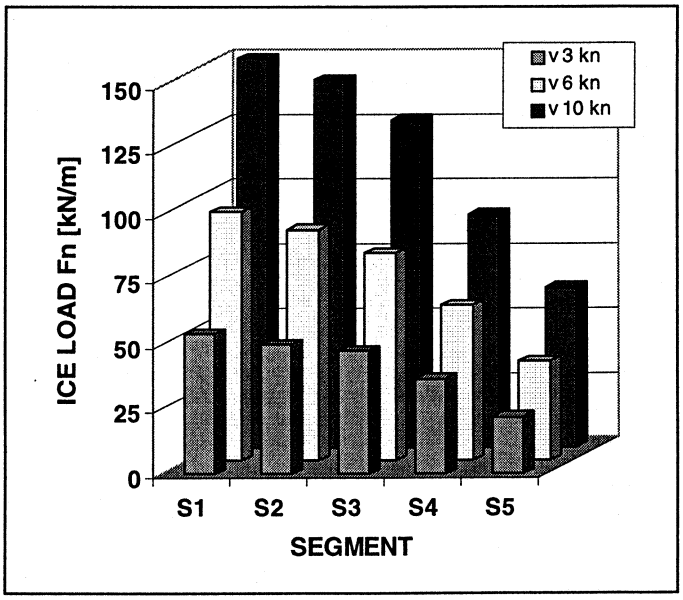

Fig. 8 Computed ice loads on the DWL with different speeds in 20 cm thick level ice field.

vertical axis shows the loads as kN/m along the DWL on five segments extending from the bow (S1) to midships (S5). The diagram shows very clearly the distribution of the ice loads to be expected on the DWL with different speeds in level ice. Similar diagrams can be computed for ice thickness or other parameters.

7. CONCLUSIONS

The computed results can be directly used to give guidelines for vessels occasionally traveling in ice covered waters on how to proceed with safety. Examples of such vessels are many naval, governmental, and commercial vessels traveling in relatively light or moderate ice conditions under limited duration of time.

Long term ice loads, on the other hand, depend strongly on the statistical variation of the ice parameters and on the operational profile of the vessel. Maximum ice loads encountered by the ship are not a result of a divine act, but a result of a (rare) momentary combination of the environmental and operational parameters of the ship leading into an extreme load case. In order to provide a more rigorous basis for the prediction of ice loads and for development of the ice rules of classification societies or national authorities, specially the dependency of the ice loads on the ship hull form, speed (or motion), ice thickness and strength parameters need to be known. The numerical results presented show that this is well possible for level ice conditions.

ACKNOWLEDGEMENTS

Special thanks are due to Mr. A. Dagnevik, Swedish Coast Guard, who made the line drawings of the KBV-181 available for this study. The financial support of the German Ministry of Research and Education (BMBF) is gratefully acknowledged.

REFERENCES

Dagnevik, A., 1998. Technical Director, Swedish Coast Guard, Personal communication.

Kivimaa, S., 1993. Long-Term Ice Load Measurements with an Ice Load Panel on Board the Cutter M.S. Uisko, Proceedings of the 12th Int. Conference on Port and Ocean Engineering under Arctic Conditions, Vol. 1, Hamburg, pp. 338-347.

Kujala, P., 1994. On the Statistics of Ice Loads on Ship Hull in the Baltic. Acta Polytechnica Scandinavica, Mech. Eng. Series. No. 116, 98 p. Finnish Acad. of Technology, Helsinki.

Thompson, J.F., Warsi, Z.U., and Mastin, C.W., 1985. *Numerical Grid Generation – Foundations and Applications.* New-York: North-Holland.

Valanto, P., 1992. The Icebreaking problem in Two Dimensions: Experiments and Theory, *Journal of Ship Research*, 36, 4.

Valanto, P., 1993. Investigation of the Icebreaking Pattern at the Bow of the Ib Kapitan Sorokin on the Yenisei River Estuary in May 1991. Proceedings of the 12th Int. Conference on Offshore Mechanics and Arctic Engineering (OMAE), Vol. IV, Glasgow, Scotland, pp. 127-134.

Valanto, P., 1995. Numerische Untersuchung des Eisbrechwiderstandes eines Schiffes bei kontinuierlicher Bewegung im ebenen Eis. HSVA-Bericht Nr. E256/95, Hamburgische Schiffbau-Versuchsanstalt GmbH, Hamburg, 71 p.